Available online at www.sciencedirect.com

ScienceDirect

Procedia Structural Integrity 7 (2017) 101–108

Structural Integrity Procedia

www.elsevier.com/locate/procedia

3rd International Symposium on Fatigue Design and Material Defects, FDMD 2017, 19-22 September 2017, Lecco, Italy

HCF resistance of AlSi10Mg produced by SLM in relation to the presence of defects

S.Romano[a,*], S. Beretta[a], A. Brandão[b], J. Gumpinger[b], T. Ghidini[b]

[a] *Politecnico di Milano, Dipartimento di Meccanica, Via La Masa 1, I 20156 Milano*
[b] *European Space Research and Technology Centre, Keplerlaan 1, NL 2200AG Noordwijk*

Abstract

Being able to predict the fatigue resistance of parts produced by additive manufacturing (AM) is a very actual and frequent open issue. The qualification of AM structural parts needs a very costly and time consuming series of fatigue tests, on both samples and full-scale parts. A proper control of the AM process allows obtaining comparable and even better fatigue resistance than standard manufacturing. Despite this, the experimental results often show a large scatter, mostly due to the presence of defects. In this framework, this work summarizes a research activity aiming at modelling the high cycle fatigue (HCF) resistance in presence of defects, focusing on AlSi10Mg produced by selective laser melting (SLM). Two batches of samples were investigated by computed tomography (CT) and tested. A lower bound resistance curve was obtained introducing artificial defects. A fatigue crack growth simulation model based on the maximum defect size is proposed, able to estimate both the life and the scatter of the data in the fully-elastic region. Moreover, knowing the size and position of all the defects inside the samples, it was possible to foresee the defect at the origin of fatigue failure and to draw a hazard ranking based on the applied stress intensity factor.

Peer-review under responsibility of the Scientific Committee of the 3rd International Symposium on Fatigue Design and Material Defects.

Keywords: AlSi10Mg; additive manufacturing; selective laser melting; high cycle fatigue; Kitagawa diagram; probabilistic fatigue life assessment

1. Introduction

One of the main issues of AM parts is the large scatter often associated to their fatigue resistance, in particular in the HCF region (see Beretta and Romano (2017); Wycisk et al. (2013); Leuders et al. (2013)). Even though the fast and progressive improvement of the AM technology is constantly mitigating this issue, the state-of-the-art knowledge of the variables in play do not allow the definition of a robust and reliable method for structural parts qualification. This issue is often overcome by space and aerospace companies by verifying a frozen process and performing extensive test

* Corresponding author. Tel.: +39-02-2399-8248; fax: +39-02-2399-8263.
E-mail address: simone.romano@polimi.it

Peer-review under responsibility of the Scientific Committee of the 3rd International Symposium on Fatigue Design and Material Defects.
10.1016/j.prostr.2017.11.066

campaigns on specimens and full-scale parts. However, a more comprehensive physics-based material characterization would allow to simplify and speed up the qualification process, reducing at the same time the expensive experimental phase.

Most of the data dispersion can be in first instance imputed to defects and assessed adopting the Kitagawa diagram, but other sources of error are also present (e.g. microstructure, variable residual stresses, etc.), see Beretta and Romano (2017) for an overview. The main parameter affecting the fatigue properties of defected materials is the size of the maximum defect, which can be described by the $\sqrt{area}$ parameter. Romano et al. (2017b) have proposed a way to analyse the defect distribution measured by CT scans and apply statistics of extremes to successfully estimate the maximum defect size in a given volume of material. However, the defect size alone is not enough to model the problem. In fact, a common observation on various materials is that most of the failures are originating on the surface (Romano et al. (2017b); Siddique et al. (2015); Wycisk et al. (2013); Yadollahi and Shamsaei (2017)).

The goal of this paper is then understanding how to estimate the size of these crucial defects and use it to evaluate the fatigue strength and life of the parts. In detail, the results of fatigue tests have been analysed through the calculation of the stress intensity factor (SIF) adopting the $\sqrt{area}$ concept by Murakami (2002). Then, fatigue strength and life estimation have been addressed with common life prediction models (such as the ones adopted in ESACRACK/NASGRO). The combination of the two approaches for the analysis of two different AM batches has allowed to pinpoint that the quality of the AM process and the subsequent fatigue properties are controlled by extreme defects.

2. Material and experiments

The material investigated in this study is the aluminium alloy AlSi10Mg. Two series of cylindrical fatigue samples were produced by SLM on an EOS M400 powder-bed machine between 2015 and 2016. In the following, they will be referred to as batch 1 (B1) and batch 2 (B2). Two different orientations have been investigated, placing the specimen's axis parallel or perpendicular to the building direction. The will be referred to as vertical in the first case and horizontal in the latter. The manufacturing parameters adopted are reported in Romano et al. (2017b). None of the parts received any final heat treatment, however, significant residual stresses were not expected due to the platform pre-heating. A common observation for SLM is that as-built parts show a significant reduction of fatigue resistance with respect to machined ones. This reduction can be in the order of 40-50% considering a technically relevant fatigue strength of $2 \cdot 10^6$ cycles, depending on the final surface quality (see Beretta and Romano (2017); Wycisk et al. (2013); Yadollahi and Shamsaei (2017)). As the aim of this paper is the assessment of AM parts in relation to the presence of manufacturing defects, all the specimens have finally been machined.

Exactly the same manufacturing process, powder and machine have been used to produce the samples. Therefore, no remarkable differences are expected between them. However, due to the fast development of the SLM technology, the recirculating inert gas system needed to remove released gas and particles was improved in the meantime. Metallographical analyses did not reveal any evident difference between the two batches.

Preliminary micro X-ray CT scans have been performed on some samples from both batches to measure the defect population in the material. The voxel size was set to 15 μm. The process parameters adopted are reported in Romano et al. (2017b). On this base, artificial defects with a size $\sqrt{area} = 500\,\mu m$ were introduced in some samples of B1 to estimate the Kitagawa diagram. The size of the artificial defects was calculated as a 97.5% percentile of the maximum defect distribution in the gage volume. More details about this distribution will be given in section 3.2 and 3.3.

An overall number of 76 fatigue tests was performed at $R = -1$, some in HCF and some in low cycle fatigue (LCF) regimes. Among these, 36 tests belong to B1 and 40 to B2. The specimen gage dimension were: a) B1 with $d_g = 5.1 - 6\,mm$ and $l_g = 16\,mm$; B2 with $d_g = 4 - 6\,mm$ and $l_g = 13 - 16\,mm$. In the following, the focus will be only on the results of HCF and of LCF experiments under fully-elastic material response. The results of all the LCF tests performed on B1 are discussed in Romano et al. (2017a).

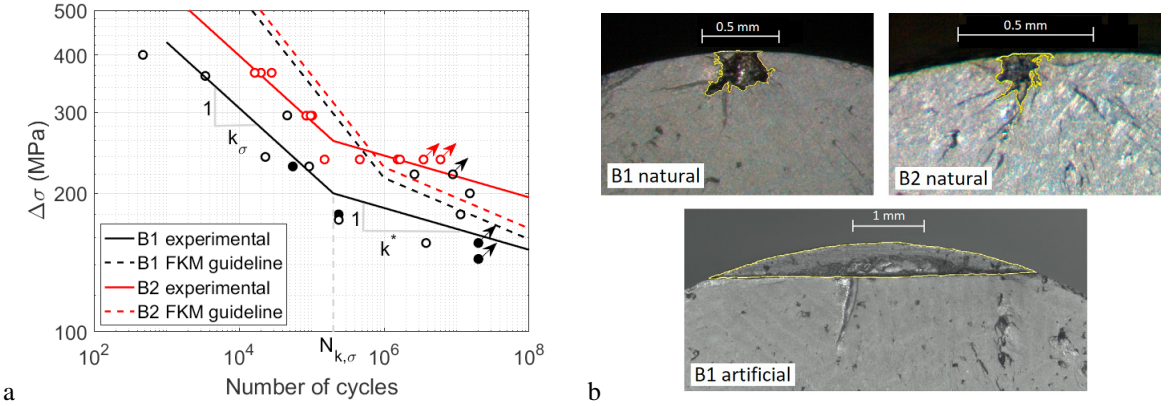

Fig. 1. HCF results for the two batches tested: (a) S-N diagrams; (b) fractographies.

3. Results

3.1. Fatigue resistance

The results of the HCF tests plus the LCF in the fully-elastic regime are summarized in Fig. 1a. As it could have been expected from the maximum defect distributions presented in section 3.2, the vertical samples generally show a slightly lower life with respect to the horizontal ones. The average difference in terms of life is less than 5% for B1, but it becomes nearly 23% considering B2. On the other hand, no visible differences were detected between vertical samples placed in different positions of the job volume. As a generic observation, the life variation due to the defect orientation is definitely negligible if compared to the one between different batches. Therefore, the whole batch has been described by a unique symbol in order to simplify the picture readability. Fig. 1b depicts examples of the defects found at the origin of failure in B1 and B2 and the shape of the artificial defects.

A first remark is that a reduction of the maximum defect size corresponds to a visibly improved fatigue resistance. At the same time, the slope of the Wöhler curves does not appear to change among the batches. For cast aluminium alloys, the FKM Guideline (2012) reports a slope $k_\sigma = 5$ before $N_{k,\sigma} = 1 \cdot 10^6$ cycles and a slope of $k^* = 15$ after this knee point. The stress value at the knee point can be estimated as 30% of the ultimate tensile strength. Fig. 1a shows that this guideline does not correctly describe the present data. In fact, the slopes are respectively $k_\sigma = 7$ and $k^* = 22$ and the change of slope happens at approximately $N_{k,\sigma} = 2 \cdot 10^5$ cycles. This deviation from the standard properties of aluminium alloys is not surprising looking at other literature results for the same material produced by SLM. Brandl et al. (2012), for example, reports a k_σ similar to the one proposed by FKM, but a knee point at $N_{k,\sigma} = 2 \cdot 10^5$ cycles as in the present case. The results by Mower and Long (2015), instead, show a slope k_σ close to 6.2, not far from this paper's results. Finally, it is worth noticing that the k^* values determined within this work are the same, as used by Sonsino (2007) and Sonsino and Franz (2017) for similar cast materials. Summarizing, predicting the fatigue life of this material without an extensive testing campaign can be a complex task, and the Wöhler curve slopes can change from one batch to another. Considering the long-life region, the fatigue strength at 20 million cycles ranges between 150 MPa and 240 MPa. Designing using safety factors could become impossible when dealing with such a large scatter. Therefore, a proper definition of the Kitagawa diagram is needed to reduce the uncertainty. This topic will be deepened in section 4.1.

Finally, it is worth observing that a large maximum defect size involves a sensible increment of the experimental scatter, both at high and low applied stresses. Describing the real variability of B1 in the whole $\Delta\sigma$ range, for example, could require a large amount of specimens and time. The artificial defects introduced in this batch give a conservative assessment of the lower bound of the data in the long-life region. For these reasons, the possibility to easily assess a lower bound resistance introducing an artificial defect in the samples appears promising to simplify, shorten and reduce the cost of material testing campaigns.

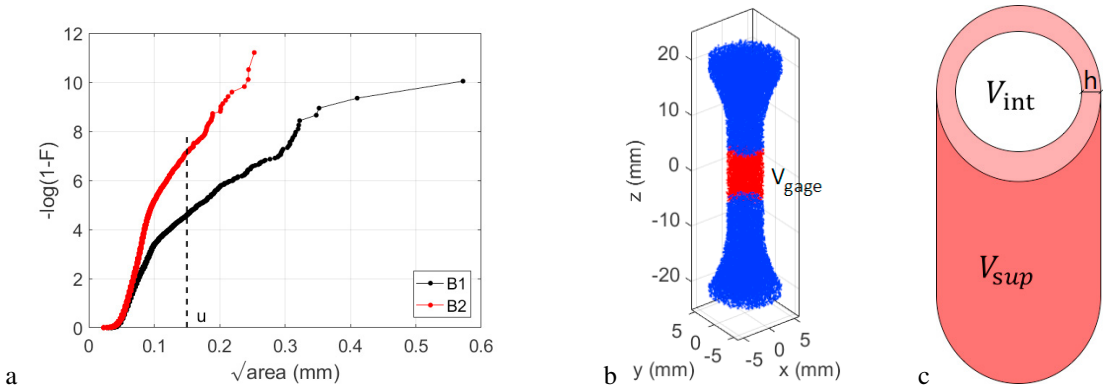

Fig. 2. CT analysis of the specimens: (a) negative exponential probability plot showing the defect distribution related to one vertical specimen for every batch; (b) defects detected inside the gage volume and grips of a sample; (c) scheme of a fictitious surface gage volume.

3.2. CT scan

The CT results have been analysed following the path described in Romano et al. (2017b). Fig. 2a shows completely different defect distributions among the two batches.

The main observations are here summarized:

- the overall number of defects detected is of the same order of magnitude, but there has been a massive reduction of the maximum defect size from B1 to B2;
- both distributions show a change of slope size at approximately 100 μm. B1 has larger defects due to a smaller slope of the data over this threshold;
- small changes in the manufacturing conditions (in this case the use of a new recirculating inter gas system) can involve important differences in the defect distribution. The fast technological growth in the field is rapidly improving material quality;
- halving the maximum defect size should involve a visible increase of the fatigue resistance from B1 to B2.

In section 1, it has been introduced that the fatigue resistance does not depend on the overall defect distribution, but on the distribution of the maximum defect. Romano et al. (2017b) have proposed a method to obtain this distribution applying a peaks-over threshold maxima sampling to the data and fitting a negative exponential distribution on the exceedances. The same method has been applied here on the various batches and orientations, setting a threshold $u = 150\ \mu m$. Considering the specimen orientation, the defect distributions are only slightly changing between horizontal and vertical samples, with the latter being more detrimental because of a defect elongation perpendicular to the stress direction, as highlighted by Romano et al. (2017b) and in accordance with the experimental life. The difference appears very small in B1 and more pronounced in B2. A quantitative evaluation of this difference is reported in section 3.3. In both batches, no remarkable differences were detected in the vertical samples placed at different distance from the platform.

3.3. Stress intensity factor at the fracture origin

After fatigue testing, the fracture surfaces of all the samples have been analysed under the microscope (see an example in Fig. 1b) and the $\sqrt{area}$ of the defect from which the failure originated (from now on called *killer*) was measured. The first evidence from this investigation is that almost all the failures originated from surface or sub-surface defects, as a confirmation of the literature evidence discussed in section 1. This happened in all but two samples, both belonging to B1 and having very large areas of lack of fusion. Looking at the CT scan results, there are no data supporting the evidence of larger defects close to the surface. On the contrary, the spatial distribution of the defects appears to be homogeneous. This suggests that the detrimental effect of defects is not only due to their size,

but also to their distance from the surface (Romano et al. (2017b)). An empirical rule by Murakami (2002) classifies a defect as superficial when Eq. 1 is verified.

$$a/h < 0.8 \tag{1}$$

When dealing with fracture mechanics, what matters is not only the stress or the crack size, but the energy that makes the crack propagate. This energy is expressed by the SIF range ΔK. Treating defects as short cracks, this quantity can be assessed according to Eq. 2, where $\Delta\sigma$ is the stress range applied on the defect.

$$\Delta K = Y \cdot \Delta\sigma \sqrt{\pi \sqrt{area}} \tag{2}$$

The influence of the defect position is given by the shape function Y. According to Murakami (2002), its value can be set to 0.5 for embedded defects or 0.65 for surface ones. This means that a surface defect has a 30% larger SIF than an embedded one.

In section 3.2, it was pointed out that the defect distribution inside the material can vary between two manufacturing jobs, even adopting the same process parameters. If the estimation of the killer defect size distribution is not an easy task when a complete CT scan of all the parts is available, this is even more complicated in all the cases in which performing a proper CT characterization is not possible. For instance, this can happen when there is no possibility to check all the parts or because some complex shapes cannot be completely scanned with an appropriate resolution. In this cases, it becomes useful to assess the killer size with a probabilistic approach, performing CT on some representative witness samples and applying statistics of extremes. As the 89% of the failure started from surface, the size of the killer defect in a sample can be estimated as the size of the maximum defect in an equivalent surface gage volume V_{surf}, as depicted in Fig. 2b-c. V_{surf} is an external circular crown having a fixed thickness h. Considering cylindrical specimens, it can be calculated using Eq. 3, where the thickness $h = \bar{a}/0.8$ is derived from Eq. 1 and $\bar{a}$ is the average experimental radius of the killers measured in those samples. The results for the material investigated are summarized in Tab. 1.

$$V_{surf} = V_{gage} - V_{int} = \pi \cdot l_g \cdot (r_g^2 - (r_g - h)^2) \tag{3}$$

Table 1. Surface volume calculation and Gumbel parameters estimation for the samples investigated.

Batch	Orientation	$\bar{a}$ (mm)	h (mm)	V_{gage} (mm^3)	V_{sup} (mm^3)	λ (mm)	δ (mm)
B1	H	0.151	0.189	452	55	0.260	0.040
B1	V	0.150	0.187	452	55	0.279	0.048
B2	H	0.074	0.092	452	27	0.171	0.021
B2	V	0.129	0.161	452	47	0.181	0.031

Applying statistics of extremes considering only the dimension of the defects, one would expect most of the failures to originate from the internal volume of the sample, as depicted in the Gumbel probability plot of Fig. 3a. On the contrary, this is not the case when the SIF distribution is considered, see Fig. 3b. The failure origin can therefore be explained by a probabilistic competing-risk assessment between the maximum SIF distributions in the surface and embedded gage volumes.

The estimates based on statistics of extremes applied to the surface gage volume are correctly describing the experimental killer size, which have been approximated by a Gumbel distribution. The model provides correct estimates even considering B2. This method to estimate the killer defect size is the base for the determination of the initial crack size in the fatigue crack growth propagation, which is the topic of section 4.

4. HCF life prediction

4.1. Kitagawa diagram

As introduced in section 3.1, AM data often shows a large scatter in the fatigue strength after the knee-point of the Wöhler curve. Most of this variability is due to the presence of defects, and it can be accounted adopting the

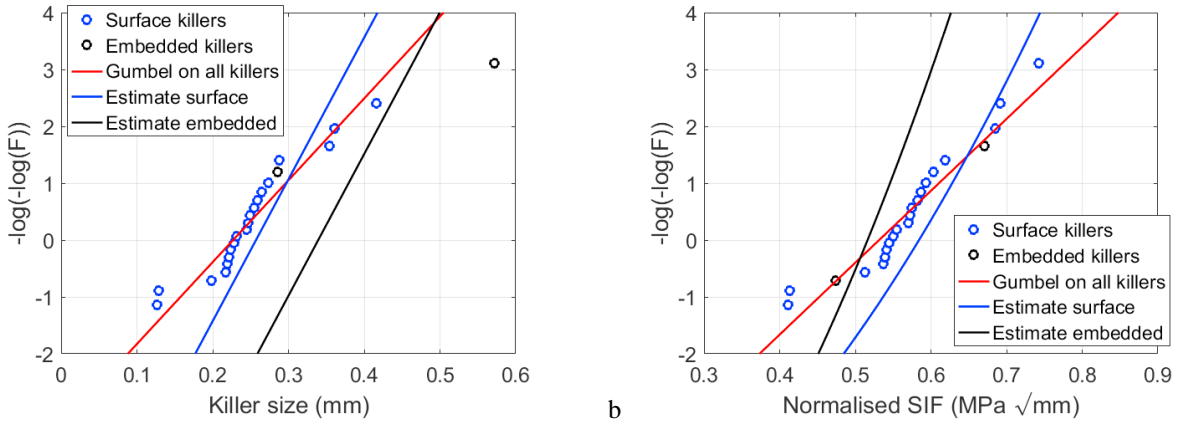

Fig. 3. Gumbel probability plot for experimental and estimated killer defect distributions for B1 considering surface and internal gage volumes: (a) defect size; (b) SIF for a unitary applied $\Delta\sigma$.

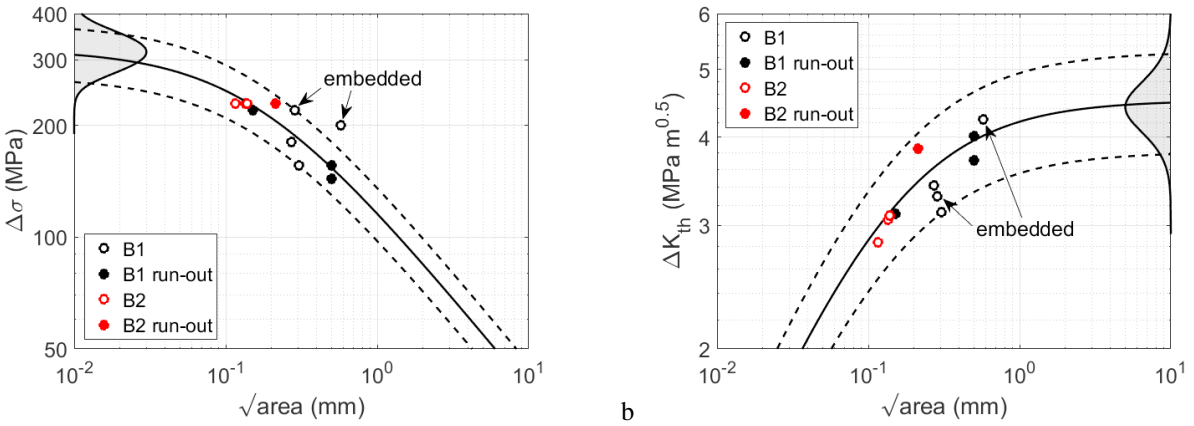

Fig. 4. Kitagawa diagram of the material described by El-Haddad formulation, fitted on B1: (a) fatigue strength over $N_{k,\sigma}$ cycles; (b) fatigue crack propagation threshold for short cracks.

Kitagawa diagram (see Beretta and Romano (2017)). This relationship was determined from all the samples of B1 that survived $N_{k,\sigma}$ cycles. The error introduced considering failures at different number of cycles is mitigated by the fact that the Wöhler curve in this region has a very high slope k^*. The introduction of artificial defects helps improving the description in a wider defect size range. The formulation by El Haddad et al. (1979) was adopted and the two fitting parameters resulted $\sqrt{area}_0 = 0.15$ mm and $\Delta\sigma_{w0} = 320$ MPa. Note that $\Delta\sigma_{w0}$ represents the fatigue limit in absence of defects, and it is therefore an upper limit for the technological improvement for a given microstructure. The best fit is depicted in Fig. 4a, showing that the fatigue results scatter can be sensibly reduced applying these concepts. The same diagram is shown in Fig. 4b in terms of crack propagation threshold ΔK_{th}. Note that Fig. 4a is valid only for surface cracks, as the applied stress should be rescaled when dealing with embedded killers. In Fig. 4b, instead, the different position is already accounted by the Y term in the SIF assessment. Therefore, also the embedded defects are described by a unique Kitagawa diagram. Finally, this alloy shows a non-negligible intrinsic scatter, which can be due to several factors (e.g. heterogeneous microstructure, anisotropy, residual stresses, errors in the testing and measuring phase). The resulting coefficient of variation is in the order of 10%.

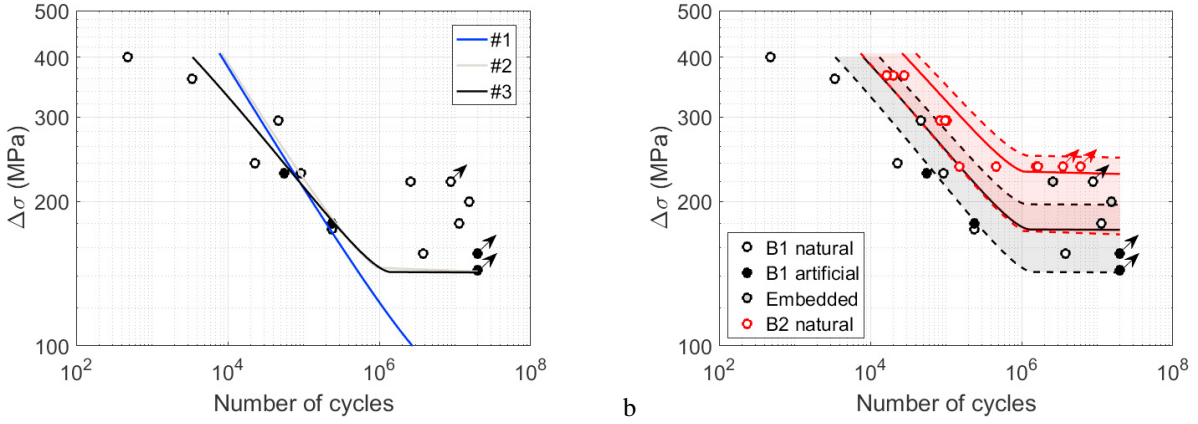

Fig. 5. HCF life estimates: (a) lower bound for B1 adopting the three options presented; (b) option #3 applied to the two batches with their 95% scatter band.

4.2. Fatigue crack growth simulation

Fatigue crack growth simulations have been performed using the software Nasgro 4.0 and a crack propagation algorithm developed for this project. The stress intensity factor was calculated adopting the standard solution for a surface crack propagating in a rod, the crack size being described only by its depth a. The diameter of the rod equals the gage one of the sample geometry investigated. Approximating the defect shape with a semi-circle, the initial crack depth a_i depends on the killer size $\sqrt{area}_i$ by the relation reported in Eq. 4, where $\sqrt{area}_i$ can be determined as a given percentile of the maximum defect distribution in the surface gage volume, as described in section 3.3.

$$a_i = \sqrt{area}_i \cdot \sqrt{2/\pi} \tag{4}$$

The $\Delta K - da/dN$ curve is described by a NASGRO equation, whose parameters were derived by fatigue crack growth tests on compact tension specimens from B1, performed in absence of crack closure (at a stress ratio $R = 0.7$). The similar slopes in the Wöhler curves of the two batches, together with the results of Fig. 4b, suggest that the fatigue crack growth properties should not be remarkably different, so the same equation has also been adopted for B2.

The life prediction was carried out under different hypotheses:

#1 - crack opening stress is calculated with the Newman model, with $\sigma_{max}/\sigma_o = 0.3$, a constraint factor $\alpha = 1.9$ and $\sqrt{area}_o = 0.038\,mm$ (standard assumptions in ESACRACK/NASGRO/AFGROW);
#2 - crack opening stress is calculated with the Newman model ($\sigma_{max}/\sigma_o = 0.3$, $\sqrt{area}_o = 0.15\,mm$ as determined from Kitagawa diagram);
#3 - crack opening stress is calculated with the Newman model (real applied σ_{max}/σ_o, $\sqrt{area}_o = 0.15\,mm$ and implementation of *plasticity corrected* crack size suggested by Newman et al. (1999).

The results of the simulations for B1 considering an initial crack size equivalent to the maximum defect (97.5% percentile) are depicted in Fig. 5a and they clearly show that conventional assumptions do not provide good results. On the contrary, option #3 provides a good estimation of the slope with an estimated value $k_\sigma = 7.5$ very close to the experiments. This highlights the importance of the *elasto-plastic* conditions for a correct analysis of the AM defects.

Fig. 5b shows the results for the two batches considering the simulation scheme #3. The dispersion of initial crack size was assessed selecting respectively the 2.5% or 97.5% percentile of the maximum defect distribution in the surface gage volume. The results confirm a good prediction together with a clear demonstration that the defect size is the key factor in fatigue properties of AlSi10Mg manufactured by AM. It is also worth remarking that there are other sources of scatter besides the initial crack size (e.g. fatigue crack growth curve, final defect size, intrinsic material scatter), which could be assessed with a fully-probabilistic model to obtain more precise and conservative results.

5. Conclusions

In this paper, the fatigue of AlSi10Mg manufactured by SLM was analysed, highlighting the role of manufacturing defects. The significant results of the activity are:

- defects are responsible for most of the experimental variability and a sensible improvement of fatigue properties can be achieved by reducing the maximum defect size;
- most of the failures are originated by surface defects since their SIF is larger than the one of internal defects. Considering the *surface volume*, the size of the defects at the fracture origin can be well estimated from CT scans measurements;
- a safe fatigue life assessment can be determined introducing artificial defects having a dimension dependent on the defect population in the material;
- a good description of the experimental results can be obtained through fatigue crack growth simulations implementing the concepts of 'plasticity corrected' crack size. Considering the initial defect size as the only source of variability, the scatter of the data is well approximated.

Acknowledgements

The activity of S. Romano has been supported by ESA through the Networking Partnering Initiative (NPI). We also acknowledge the support of RUAG, in particular Dr. M. Gschweitl, for manufacturing the specimens and for permission to publish results.

References

Beretta, S., Romano, S., 2017. A comparison of fatigue strength sensitivity to defects for materials manufactured by AM or traditional processes. Int. J. Fatigue 94, 178–191. doi:http://dx.doi.org/10.1016/j.ijfatigue.2016.06.020.

Brandl, E., Heckenberger, U., Holzinger, V., Buchbinder, D., 2012. Additive manufactured AlSi10Mg samples using Selective Laser Melting (SLM): Microstructure, high cycle fatigue, and fracture behavior. Mater. Des. 34, 159–169. doi:10.1016/j.matdes.2011.07.067.

El Haddad, M.H., Topper, T.H., Smith, K.N., 1979. Prediction of non propagating cracks. Engineering Fracture Mechanics 11, 573–584. doi:10.1016/0013-7944(79)90081-X.

FKM Guideline, 2012. Analytical strength assessment of components in mechanical engineering. 6th, rev. ed., VDMA-Verl.

Leuders, S., Thöne, M., Riemer, A., Niendorf, T., Tröster, T., Richard, H.A., Maier, H.J., 2013. On the mechanical behaviour of titanium alloy TiAl6V4 manufactured by selective laser melting: Fatigue resistance and crack growth performance. Int. J. Fatigue 48, 300–307. doi:10.1016/j.ijfatigue.2012.11.011.

Mower, T.M., Long, M.J., 2015. Mechanical Behavior of Additive Manufactured, Powder-bed Laser-Fused Materials. Mater. Sci. Eng. A 651, 198–213. doi:10.1016/j.msea.2015.10.068.

Murakami, Y., 2002. Metal Fatigue: Effects of Small Defects and Nonmetallic Inclusions. Elsevier, Oxford.

Newman, J., Phillips, E.P., Swain, M., 1999. Fatigue-life prediction methodology using small-crack theory. International Journal of fatigue 21, 109–119.

Romano, S., Beretta, S., Foletti, S., 2017a. LCF response of AlSi10Mg obtained by Additive Manufacturing, in: Eighth International Conference on Low Cycle Fatigue (LCF8), Dresden.

Romano, S., Brandão, A., Gumpinger, J., Gschweitl, M., Beretta, S., 2017b. Qualification of AM parts: extreme value statistics applied to tomographic measurements. Materials & Design , 1–34.

Siddique, S., Imran, M., Rauer, M., Kaloudis, M., Wycisk, E., Emmelmann, C., Walther, F., 2015. Computed tomography for characterization of fatigue performance of selective laser melted parts. Mater. Des. 83, 661–669. doi:10.1016/j.matdes.2015.06.063.

Sonsino, C.M., 2007. Course of SN-curves especially in the high-cycle fatigue regime with regard to component design and safety. International Journal of Fatigue 29, 2246–2258. doi:10.1016/j.ijfatigue.2006.11.015.

Sonsino, C.M., Franz, R., 2017. Multiaxial fatigue assessment for automotive safety components of cast aluminium EN AC-42000 T6 (G-AlSi7Mg0.3 T6) under constant and variable amplitude loading. International Journal of Fatigue 100, 489–501. doi:10.1016/j.ijfatigue.2016.10.027.

Wycisk, E., Emmelmann, C., Siddique, S., Walther, F., 2013. High Cycle Fatigue (HCF) Performance of Ti-6Al-4V Alloy Processed by Selective Laser Melting. Adv. Mater. Res. 816-817, 134–139. doi:10.4028/www.scientific.net/AMR.816-817.134.

Yadollahi, A., Shamsaei, N., 2017. Additive Manufacturing of Fatigue Resistant Materials: Challenges and Opportunities. Int. J. Fatigue 98, 14–31. doi:10.1016/j.ijfatigue.2017.01.001.